Journal of Power Sources 229 (2013) 48–57

Contents lists available at SciVerse ScienceDirect

Journal of Power Sources

journal homepage: www.elsevier.com/locate/jpowsour

Performance and stability of proton conducting solid oxide fuel cells based on yttrium-doped barium cerate-zirconate thin-film electrolyte

Yeong Yoo*, Nguon Lim [1]

Energy, Mining, and Environment (EME) Portfolio, National Research Council Canada, Ottawa, ON, Canada K1A 0R6

HIGHLIGHTS

- ► Fabricated thin-film BCZY-based high performance anode supported SOFCs by wet powder spraying.
- ► Clarified nickel diffusion and its effect on the co-sintering of BCZY supported on Ni cermet anode.
- ► Demonstrated the highest power density in high temperature proton conducting planar cells.
- ► Demonstrated high performance reversible SOFCs comprising of thin-film BCZY and BSCF cathode.
- ► Investigated the chemical stability of BCZY in water-containing atmosphere for practical applications.

ARTICLE INFO

Article history:
Received 20 August 2012
Received in revised form
23 November 2012
Accepted 24 November 2012
Available online 30 November 2012

Keywords:
Yttrium-doped barium cerate-zirconate
Proton conducting SOFCs
Stability
Thin-film electrolyte
Reversible SOFCs

ABSTRACT

The high performance anode supported single cells, comprising of BSCF ($Ba_{0.5}Sr_{0.5}Co_{0.8}Fe_{0.2}O_{3-\delta}$)-BCZY ($Ba_{0.98}Ce_{0.6}Zr_{0.2}Y_{0.2}O_{3-\delta}$)//BCZY//NiO–BCZY have been fabricated by wet powder spraying and co-firing for depositing 10–15 μm thin film electrolytes on pre-sintered NiO–BCZY anode discs. The open circuit voltages of single cells were around 1.12–1.13 V at 600 °C indicating negligible gas leakage or mixed conduction through the electrolyte. The maximum power density of 493 mW cm^{-2} was obtained at 600 °C and 0.7 V under humid air as the oxidant gas and humid 75% H_2 in N_2 (2.76% H_2O) as the fuel gas at a gas flow rate of 100 ml min^{-1}. The area specific resistance of an anode supported button cell of BSCF–BCZY//BCZY//NiO–BCZY in fuel cell mode was about 0.46 Ω cm^2 and in the electrolysis mode was 0.26 Ω cm^2 at 600 °C, indicating high efficiency, reversible SOFCs. The single cell performance was stable for over 600 h at 600 °C. The stability of BCZY electrolyte in water-containing atmospheres was investigated by exposing sintered BCZY pellets to humid air (2.76% H_2O) at 200 °C for 24 h or soaking them in boiling water for 3 h.

1. Introduction

High temperature proton conducting solid electrolytes based on perovskite-type oxides such as doped $SrCeO_3$, $BaCeO_3$, and $SrZrO_3$ have been investigated for a variety of applications such as fuel cells, steam electrolysis, hydrogen separation, and hydrogen sensors [1–5]. Even if Gd-doped $BaCeO_3$ exhibits the highest conductivity of 2×10^{-2} S cm^{-1} at 600 °C among the proton conducting electrolytes stable in a fuel cell environment [6,7], it was reported that $BaCe_{0.8}Gd_{0.2}O_{3-\delta}$ (BCG) has severe diffusion of nickel from NiO–BCG anode during co-firing the bilayer of NiO–BCG anode and BCG electrolyte, resulting in forming a high temperature liquidus phase of Ba–Ni–O and a segregated solid phase of gadolinium- and nickel-rich Ba–Ce–O [8] and reducing the ionic conductivity of BCG electrolyte and open circuit voltages of BCG-based single cells [9]. In addition, it is well known that $BaCeO_3$ has thermodynamic instability under CO_2-containing atmosphere of P_{CO_2} = 1.0 atm at temperatures below 1090–1185 °C [10–12] and H_2O-containing atmosphere of P_{H_2O} = 0.57 atm at temperatures below 900 °C [13] or P_{H_2O} = 0.5 atm at temperatures below 492 °C [14], depending on the different sets of thermodynamic data used. Bhide and Virkar reported that undoped, Gd-doped, and La-doped $BaCeO_3$ ceramics at all dopant levels were readily decomposed within a few hours when boiled in water and some of the powders were decomposed when heated in moist air at 200 °C after several days of exposure [15]. Regardless of the contradictory thermodynamic calculation on the boundary condition for thermodynamically stable temperatures, the stability of $BaCeO_3$ under H_2O-containing atmosphere at

* Corresponding author. Tel.: +1 613 993 5331; fax: +1 613 991 2384.
E-mail address: yeong.yoo@nrc-cnrc.gc.ca (Y. Yoo).
[1] Current address: Ottawa, ON, Canada.

0378-7753/$ – see front matter
http://dx.doi.org/10.1016/j.jpowsour.2012.11.094

low temperatures would be much more critical for practical applications because of inevitable thermal cycling during the long term operation of devices such as fuel cells.

In order to enhance the chemical stability of $BaCeO_3$, solid solutions between cerate and zirconate have been considered because barium zirconate is stable in CO_2-containing atmosphere, but has relatively low proton conductivity [16–18]. From these investigations, it was demonstrated that the introduction of Zr into doped barium cerate greatly enhanced its chemical stability, but the incorporation percentage of Zr required for sufficient chemical stability depended on the trivalent element doped to B site in ABO_3-type perovskite of doped barium cerate zirconate for introducing oxygen ion vacancy. It was also reported that the Zr content in the range 20–40 mol% in doped barium cerate zirconate would be required to maintain high electrical conductivity and chemical stability under CO_2-containing atmosphere [19,20]. Yttrium doped barium cerate zirconate ($BaCe_{1-x-y}Zr_xY_yO_{3-\delta}$, BCZY) in the form of sintered pellets has been widely investigated as one of promising proton conducting materials with high conductivity and chemical stability under CO_2- or H_2O- or H_2S-containing atmosphere [20–25]. Among barium cerate zirconate compounds of $BaCe_{0.45}Zr_{0.45}M_{0.1}O_{3-\delta}$ (M = In, Y, Gd, Sm) doped with one of four aliovalent rare earth elements of In, Y, Gd and Sm, Y-doped barium cerate zirconate exhibited the highest conductivity, resulting from the similarity between the effective ionic radii of Ce^{4+} (0.87 Å) and Y^{3+} (0.90 Å) with the coordination number of 6 [25,26]. In addition, the single cell performance of thick- or thin-film BCZY electrolyte-based SOFCs has been also demonstrated to explore the potential use of BCZY proton conducting material for hydrogen or ammonia fuelled intermediate temperature SOFCs and reversible SOFCs [27–32], but there is still a lack of detailed information for the maximum achievable power density at intermediate temperatures using thin-film proton conducting electrolyte, long term durability and performance degradation during thermal cycling under humid gas atmosphere.

In this paper, high performance anode supported single cells, comprising of BSCF ($Ba_{0.5}Sr_{0.5}Co_{0.8}Fe_{0.2}O_{3-\delta}$)-BCZY composite cathode, BCZY ($Ba_{0.98}Ce_{0.6}Zr_{0.2}Y_{0.2}O_{3-\delta}$) electrolyte containing 20 mol% Zr and 20 mol% Y in B site, and NiO–BCZY anode have been fabricated by wet powder spraying and co-firing for depositing 10–15 μm thin film electrolytes on pre-sintered NiO–BCZY anode discs for a variety of applications such as humid hydrogen or potentially ammonia fuelled proton conducting SOFCs and high temperature steam electrolysis as reversible SOFCs. The electrochemical performance and durability of single cells were characterized at the temperature 600–700 °C under humid 50–75% H_2 in N_2 (2.76% H_2O) as the fuel gas and humid air as the oxidant gas at a gas flow rate of 10–100 ml min^{-1}. In addition, the electrochemical performance of single cells under electrolysis mode was also characterized at 600 °C for confirming potential production of hydrogen via high temperature steam electrolysis using BCZY thin film electrolyte-based single cells. The stability of BCZY electrolyte in water-containing atmospheres was investigated by exposing sintered BCZY pellets to humid air (2.76% H_2O) at 200 °C for 24 h or soaking them in boiling water for 3 h in order to enhance understanding about potential problematic degradation issues during thermal cycling under humid gas atmosphere.

2. Experimental

2.1. Preparation of anode supported half cells with thin-film BCZY electrolyte

Porous NiO–BCZY substrates were fabricated by conventional powder pressing and sintering methods. The mixture of 60 wt.% NiO (J. T. Baker) and 40 wt.% $Ba_{0.98}Ce_{0.6}Zr_{0.2}Y_{0.2}O_{3-\delta}$ (d_{50} 1.2 μm, 6.3 m^2 g^{-1}, Praxair) powders was ball-milled for 2 h in ethanol and dried at 85 °C. The dried mixture was sieved and mixed with 3–10 wt.% graphite for adjusting sintering shrinkage and then pressed under 40 MPa with 20 mm in diameter and 0.8 mm in thickness. The pressed pellets of NiO–BCZY were pre-sintered in air at 700 °C for 2 h. The proton conducting oxide electrolyte layer of BCZY with 10–15 μm was deposited on the pre-sintered NiO–BCZY anode substrates by pulsed injection type wet powder spraying developed at the National Research Council of Canada (NRC) [33]. The mixture of 90 wt.% ethanol and 10 wt.% deionized water was used for controlling the evaporation speed of the suspension medium during wet spraying, and its powder loading was set at about 1.0 g per 10 ml of suspension. The deionized water–ethanol-based suspension containing BCZY was prepared by high-energy ball milling (SPEX CertPrep, USA) for 1 h and sprayed on the pre-sintered NiO–BCZY anode pellets. The resulting bi-layers were sintered at 1300–1400 °C in air for 2 h.

2.2. Synthesis and deposition of BSCF cathode

As starting materials, $BaCO_3$, $SrCO_3$, Co_3O_4 and Fe_2O_3 powders were used to synthesize $Ba_{0.5}Sr_{0.5}Co_{0.8}Fe_{0.2}O_{3-\delta}$ (BSCF) via conventional solid state reaction. Mixtures of the starting materials were ground and calcined in air at 1000 °C for 3 h. They were then reground, pressed into pellets and sintered in air at 1050 °C for 2 h. BSCF powders synthesized by solid state processing were used for preparing cathodes on anode-supported half cells with thin-film BCZY electrolyte. The ethanol-based powder suspensions of BSCF or BSCF–BCZY (70:30 wt.%) were prepared by high energy ball milling for 20 min and sprayed on the sintered bi-layer of BCZY electrolyte and NiO–BCZY anode by the pulsed injection type wet powder spraying. The cathode with 20 μm thickness and 6 mm diameter was sprayed on the sintered bi-layer and fired at 850–900 °C for 1 h in air to minimize the interfacial reaction between BCZY electrolyte and BSCF cathode for the electrochemical characterization of single cells.

2.3. Characterization

The phase formation of compounds and the chemical compatibility of synthesized BSCF with BCZY were examined by X-ray diffraction on a Bruker D8 Advanced X-ray diffractometer (Bruker AXS Gmbh, Karlsruhe, Germany) using Cu-Kα radiation by collecting the diffractogram from $2\theta = 20°–80°$ with 0.04° step size. The surface and cross-sectional microstructures and elemental determinations of bilayer half cells and single cells after the deposition of cell components or cell testing were examined by a JEOL JSM-840A scanning electron microscope (SEM) equipped with both a secondary electron (SE) and backscattered electron (BE) detector as well as an Oxford Instruments 6560 INCAx-sight light element energy dispersive X-ray (EDX) spectrometer. The spectrometer is equipped with a Si (Li) crystal and a Super Atmospheric Thin Window (SATW) that is capable of detecting Be to U at a spectral resolution of 129 eV. Spectra were collected at an accelerating voltage of 20 kV and current of 2 nA for a total live time of 45 s. X-ray maps were collected with a resolution of 256 × 256 pixels. The samples were sputtered and coated with gold for a total of 30 s to improve conductivity.

The *C–V* characteristics and degradation of single cells composed of BSCF or BSCF–BCZY//BCZY//NiO–BCZY for fuel cell and steam electrolysis modes were evaluated in the temperature range of 600–700 °C under humid 50–75% H_2 in Ar (3% H_2O) as the fuel gas and humid air as the oxidant gas at a gas flow rate of 10–100 ml min^{-1}. Impedance data were obtained at open circuit

potential using an impedance/gain-phase analyzer Solartron SI 1260 and an electrochemical interface Solartron SI 1287 (Solartron Analytical, Farnborough, UK) over a frequency range 10^{-2}–10^{6} Hz with an applied potential of 10 mV. The concentrations of O_2 and H_2 during the high temperature steam electrolysis were monitored by Ametek Proline 8 channel mass spectrometer for calculating the current efficiency to produce hydrogen from steam. In order to determine the chemical stability of BCZY electrolyte in water-containing atmospheres, BCZY pellets with 15 mm diameter and 3–4 mm thickness were sintered at 1500 °C for 2 h in air and the sintered pellets were exposed to humid air (2.76% H_2O) with a gas flow rate of 100 ml min^{-1} in a 2 inch diameter tubular furnace at 200 °C for 24 h or soaked in boiling water for 3 h. The deposit formation and its elemental analysis on the surface of sintered BCZY pellets treated in water-containing atmospheres were examined by X-ray diffraction and SEM/EDX, respectively.

3. Results and discussion

3.1. Ni diffusion from Ni cermet anode to barium cerate electrolyte during co-firing

The fabrication of an anode supported half cell with any thin-film electrolyte via co-firing requires well-matched sintering shrinkage and profile between an anode support and a thin-film electrolyte to prevent mechanical defects such as cracking, peeling and bending in the sintered electrolyte and anode. In addition, the microstructure of the anode and the electrolyte should be controlled to provide appropriate gas permeability through the anode and prevent any gas leakage through the solid electrolyte. In order to fabricate a high performance anode supported half cell with a thin-film electrolyte, the chemical diffusion from the anode support to the electrolyte should be also prevented or carefully controlled.

Agarwal et al. reported that the presence of Ni decreases ionic conductivity and increases the electronic transference number of $BaCe_{0.8}Gd_{0.2}O_{3-\delta}$ (BCG) electrolyte sintered on NiO–BCG anode support at 1200 °C, resulting in the reduced open circuit voltages and poor cell performance with the peak power density of 113 mW cm^{-2} at 800 °C [9]. It was also reported that $BaCe_{0.8}Gd_{0.2}O_{3-\delta}$ (BCG) has severe diffusion of nickel from NiO–BCG anode during co-firing at 1250 °C, resulting in forming a high temperature liquidus phase of $BaNiO_x$ and a segregated solid phase of gadolinium- and nickel-rich Ba–Ce–O with the approximate formula of $Ba_{1.0}Ce_{0.2}Gd_{1.4}Ni_{0.7}O_4$ [8] that would be practically $BaGd_2NiO_5$ [34]. Therefore, the severe Ni diffusion from Ni-based cermet anode into barium cerate electrolyte should be avoided or minimized to enhance cell performance by changing fabrication processing or cell components. Yoo et al. have demonstrated high performance anode supported $BaCe_{0.8}Y_{0.2}O_{3-\delta}$ (BCY) thin-film electrolyte cells fabricated by co-pressing and sintering [8] as well as wet powder spraying and sintering [35] with the power densities of 160 mW cm^{-2} and 400 mW cm^{-2} at 600 °C, respectively, indicating that the BCY electrolyte has much reduced Ni diffusion in comparison to the BCG electrolyte. In order to enhance the densification of doped barium cerate electrolyte supported on Ni-based cermet anode, a higher sintering temperature would be applied, but there are certain restrictions to increase the sintering temperature due to the different levels of Ni diffusion dependent on the chemical composition in the barium cerate electrolyte.

Fig. 1 shows scanning electron micrographs and EDX profiles of the fractured surface of (a) BCY//NiO–BCY and (b) BCZY//NiO–BCZY bilayers sintered at 1250 and 1350 °C, respectively. The line profile analysis was conducted by scanning the SEM electron beam along the preselected line across the fractured surface. It was determined that Ni from NiO–BCY anode diffused into BCY electrolyte to form a nickel- and yttrium-rich barium-containing oxide phase as shown in Fig. 1a, similarly with the nickel diffusion through BCG [8]. Tong et al. reported that the addition of NiO as a sintering aid to BCY and $BaZr_{0.8}Y_{0.2}O_{3-\delta}$ (BZY) pellets formed a secondary solid phase, BaY_2NiO_5 (PDF 00-041-0463) and an intermediate phase, $BaNiO_x$ during solid-state reactive sintering. The secondary phase of BaY_2NiO_5 has a relatively low melting point of around 1450 °C and enhances the densification and grain growth of barium cerate or zirconate electrolyte [36,37]. Both of BCY and BCZY sintered on Ni-based anode have Ni diffusion at the interfacial region as shown in Fig. 1, but BCZY has lower Ni diffusion than BCY.

Fig. 2 shows the secondary solid precipitates formed in grains and at the grain boundaries on the surface of BCY thin-film electrolyte on a porous NiO–BCY anode sintered at 1250 °C for 2 h in air. According to the EDX point analysis on three areas of spectrum 3, 4, and 5, the chemical formula of $Ba(Ce_{0.2}Y_{0.8})_{1.7}Ni_{0.9}O_{5.7}$ was obtained and very similar with that of BaY_2NiO_5 reported elsewhere [37]. Fig. 3 shows the EDS maps of the fractured surface of the bilayer sample sintered at 1200 °C after applying cold isostatic pressing on a presintered NiO–BCY pellet sprayed with BCY to decrease co-firing temperatures, resulting in the reduction of the Ni diffusion. The BCY electrolyte co-fired with NiO–BCY anode at an even lower temperature of 1200 °C still formed the secondary phase precipitates of yttrium-rich barium nickel oxides distributed in the layer as well as on the outer surface as shown in Fig. 3(c) and (d).

As reported for BCG electrolyte sintered on NiO–BCG by Yoo et al. [8] and for BCY and BZY electrolytes sintered with NiO by Tong et al. [36,37], it is expected that an intermediate phase, $BaNiO_x$ ($x = 2$–3, preferably 2.55) can be formed at around 800 °C in BCZY deposited on NiO–BCZY, resulting in the Eq. (1).

$$Ba(Ce_{0.6}Zr_{0.2}Y_{0.2})O_{2.9} + yNiO = yBaNiO_x + Ba_{1-y}(Ce_{0.6}Zr_{0.2}Y_{0.2})O_{2.9-\delta} \quad (1)$$

Above 900 °C, the intermediate phase disappears and a new Ni-containing phase, BaY_2NiO_5 is formed [37] as described in the Eqs. (2) and (3). Barium-deficient barium cerate created by the above chemical reaction and barium losses that happen easily at high temperatures can cause the decomposition of the perovskite [38], resulting in BaO, (Ce, Zr)O_2 and Y_2O_3 (Eq. (2)).

$$Ba(Ce_{0.6}Zr_{0.2}Y_{0.2})O_{2.9} = BaO + 0.8(Ce_{0.75}Zr_{0.25})O_2 + 0.1Y_2O_3 \quad (2)$$

$$BaNiO_2 + Y_2O_3 = BaY_2NiO_5 \quad (3)$$

As shown in Fig. 1, BCZY has higher resistance to Ni diffusion, resulting in the formation of the secondary phase of BaY_2NiO_5 than BCY at high temperatures. Therefore, it was possible to increase the sintering temperature of BCZY electrolyte deposited on NiO–BCZY anode up to 1350–1400 °C for producing dense BCZY thin-film electrolyte without the formation of any visible secondary phase on the surface as shown in Fig. 4, indicating no excessive Ni diffusion through BCZY electrolyte. This result is coincident with the rapid densification and grain growth of Y-doped barium zirconate pellets with 2 wt.% sintering aid of NiO at temperatures above 1350 °C, reported by Tong et al. [37].

3.2. Chemical compatibility of BSCF and BCZY

BSCF single phase perovskite with cubic structure was successfully synthesized at 1050 °C for 2 h via conventional solid state processing. The chemical compatibility of BSCF and BCZY at

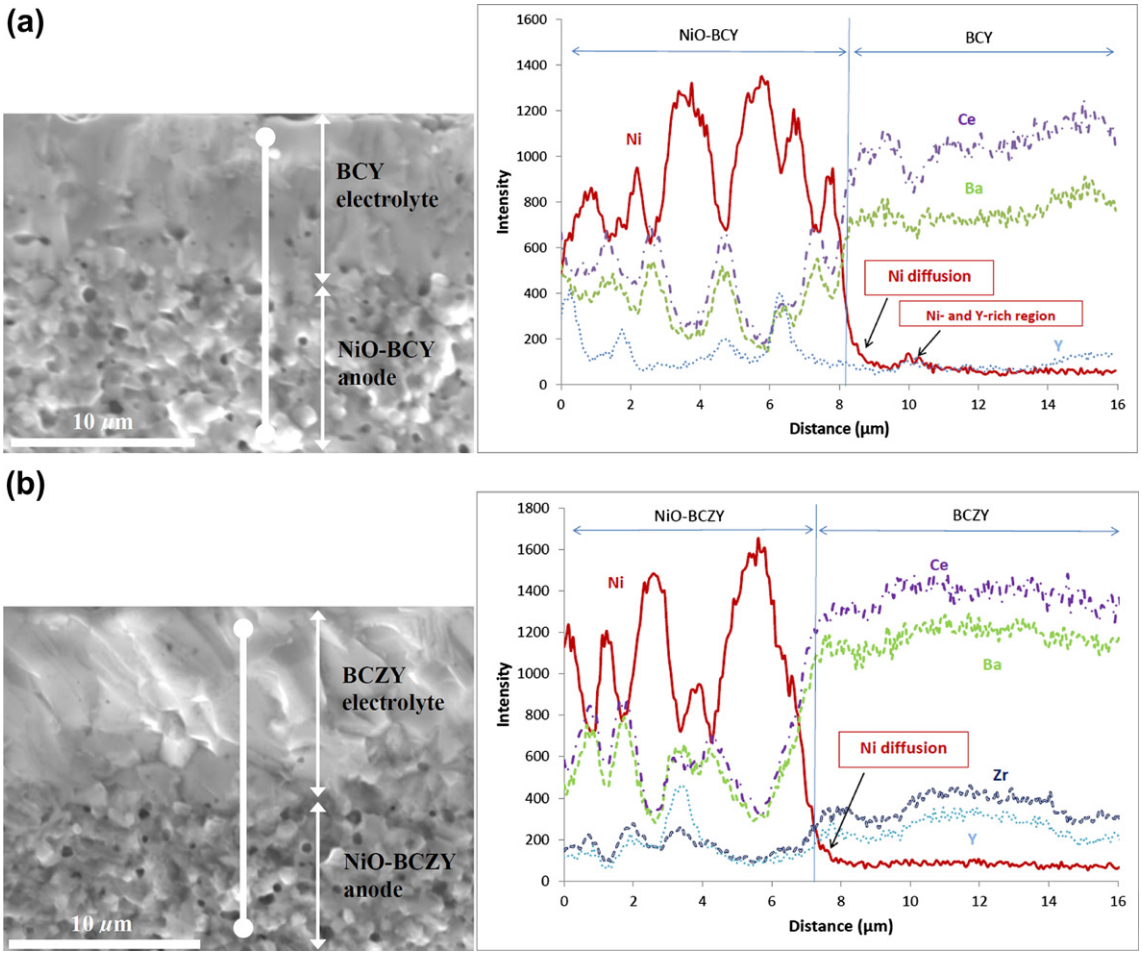

Fig. 1. Scanning electron micrographs and EDX profiles of the fractured surfaces of (a) BCY//NiO–BCY and (b) BCZY//NiO–BCZY bilayers sintered at 1250 and 1350 °C, respectively.

different temperatures was investigated in detail as shown in Fig. 5(a). In order to determine the chemical compatibility of the BSCF cathode with the BCZY electrolyte at high temperatures, the mixtures of synthesized cathodes and commercial BCZY (50:50 wt.%) powders as pressed pellets were heated up to 700–1100 °C for 10 h in air. The mixture of BSCF and BCZY heated up to 800 °C shows no significant reacted phases. However, above 900 °C, a reacted phase with peak shifts from BSCF peaks appears in the diffraction patterns, which can be attributed to chemical reactions with Ba or Y/Zr elements from BCZY.

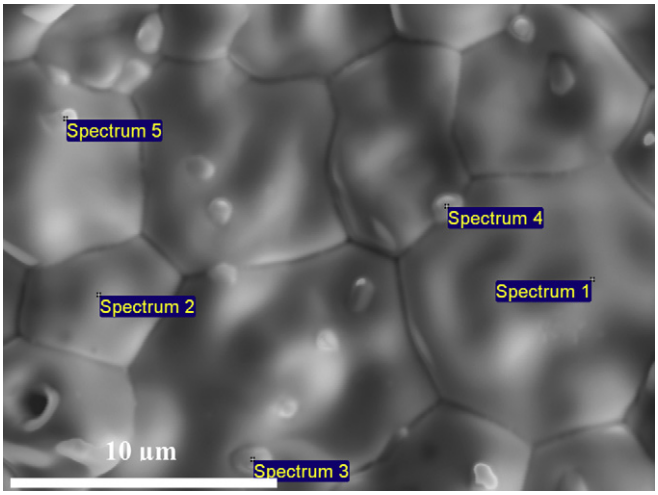

Fig. 2. Scanning electron micrographs and EDX point analysis of the surface of BCY thin-film electrolyte on a porous NiO–BCY anode sintered at 1250 °C for 2 h in air.

The synthesized BSCF has a cubic perovskite structure with the space group of *Pm3m* and is stable with no evidence of decomposition in the oxygen partial pressure range of 10^{-5}–10^{-1} atm at temperatures up to 1000 °C [39]. In addition, Wang et al. reported BSCF exhibits good phase reversibility during temperature cycling and structure stability under air up to 1000 °C [40].

As one of possible chemical reactions, the incorporation of larger ionic radius ions such as Y^{3+} and Zr^{4+} into B-site of a perovskite crystal structure can increase the average unit cell volume of the crystal [40,41]. Yttrium and zirconium in BCZY can be diffused and incorporated into BSCF in the mixture at high temperatures. The effective ionic radii of Y^{3+} (0.90 Å) and Zr^{4+} (0.72 Å) is larger than Co^{4+} (0.53 Å), Co^{3+} (0.545 Å), Fe^{3+} (0.645 Å) and Fe^{4+} (0.585 Å) with the coordination number of 6 in B-site [26,42–45].

Alternatively, Ba^{2+} in BCZY can be also incorporated into A-site of BSCF perovskite, resulting in the formation of A-site cation-rich BSCF perovskite with an increased unit cell volume. Lin et al. reported that Ba-rich BSCF formed by the diffusion of Ba^{2+} from $BaCe_{0.8}Y_{0.1}O_{3-\delta}$ into BSCF during the high temperature firing of the mixture of BSCF and $BaCe_{0.8}Y_{0.1}O_{3-\delta}$ [46]. Fig. 5(b) shows the detailed peak shifts of BCZY and BSCF heat-treated at high temperatures. The diffraction patterns of BCZY heat-treated at high temperatures over 900 °C show peak shift toward higher 2 theta, indicating a smaller unit cell volume than the stoichiometric

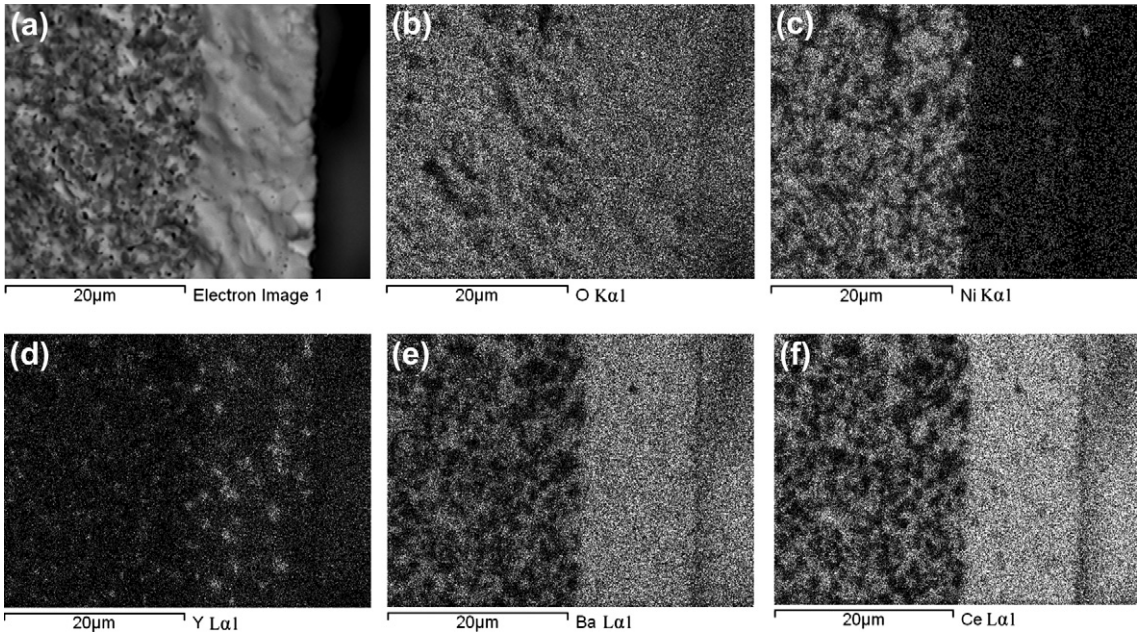

Fig. 3. SEM image (a) and EDS maps for O (b), Ni (c), Y (d), Ba (e), and Ce (f) From the fractured surface of BCY thin-film electrolyte on a porous NiO–BCY anode sintered at 1200 °C for 2 h in air.

compound, resulting from the loss of BaO at high temperatures [47]. Ba-deficient doped barium cerate formed by the loss of BaO can readily incorporate a B-site doping element with a smaller ionic radius than Ba^{2+} onto the A-site as described by the Eq. (4), resulting in the decrease of a unit cell volume [48].

$$2Ba_{Ba}^{x} + M_2O_3 + V_o^{\cdot} \rightarrow 2M_{Ba}^{\cdot} + O_o^{x} + 2BaO \quad (4)$$

where M is the trivalent dopant species. If it is assumed that Y or Zr in B-site can be also diffused to BSCF to form Y/Zr doped B-site cation-rich BSCF, the peaks of A-site cation-rich BCZY should be slightly shifted toward lower 2 theta in the diffraction patterns due to the increase of the unit cell volume [47,49].

BSCF in Fig. 5(b) shows the peak split to form another perovskite phase with lower 2 theta above 900 °C, indicating the formation of

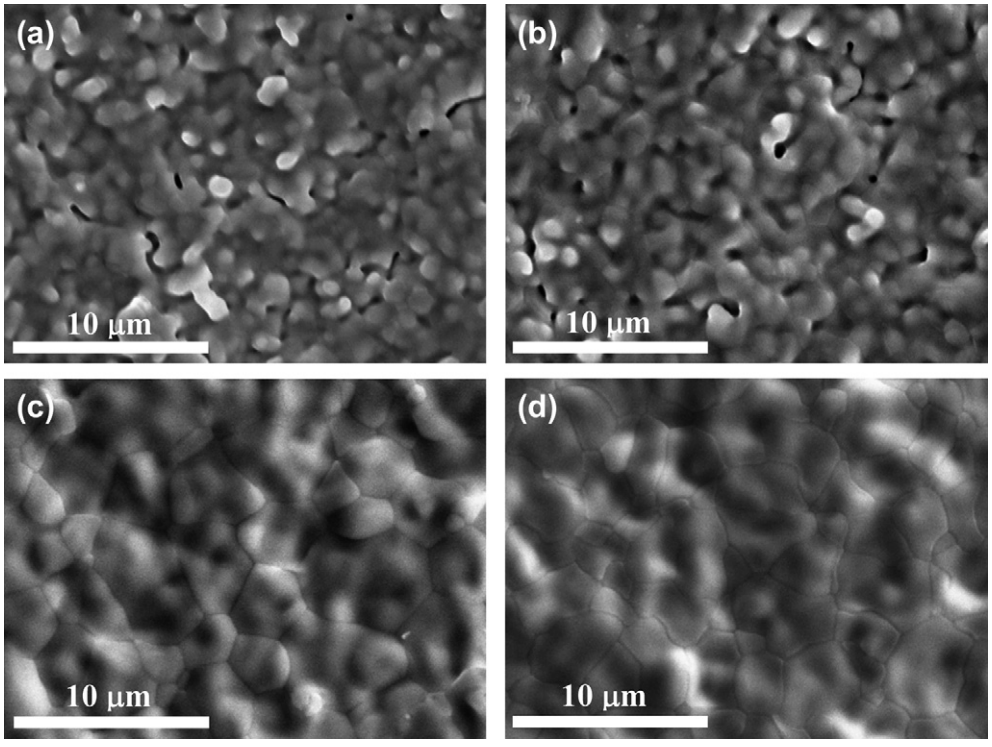

Fig. 4. SEM photos of the surface of BCZY on NiO–BCZY sintered at (a) 1300, (b) 1325, (c) 1350, and (d) 1400 °C for 2 h in air.

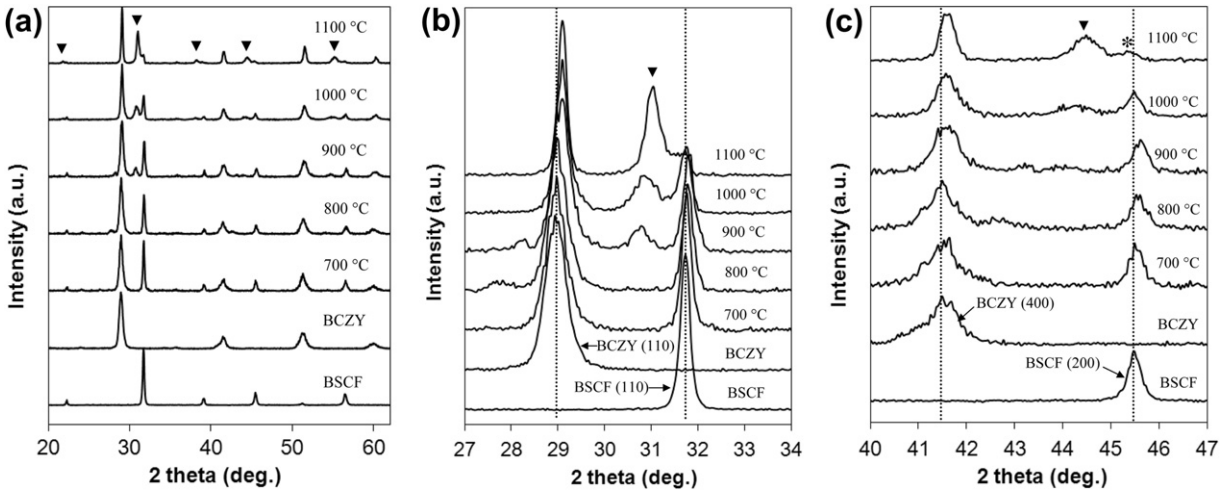

Fig. 5. XRD patterns collected over the 2-theta range of 20–62° (a), 27–34° (b), and 40–47° (c) of BSCF, BCZY and the mixture of BSCF and BCZY heat-treated at 700–1100 °C for 10 h in air (▼: $BaCoO_{2.23}$, *: Ba-rich BSCF).

a perovskite phase with a larger unit cell volume. Its lattice constant was around 4.073 Å calculated by Topas software (Version 2.0). The formed perovskite phase was identified as $BaCoO_{2.23}$ with a cubic structure (a = 4.072 Å, JCPDS 75–0227). The oxidation number of the cobalt in the perovskite is 2.46 and the cubic structure can be stabilized by increasing Co ionic size resulted from the reduction of the average valence state of cobalt and lowering the coordination number of cobalt ions by removal of some oxide ions [50]. Yang et al. also reported the formation of $BaCoO_3$ and $Sm_2Zr_2O_7$ with a mixed conductivity during the calcination of the mixture of BCZY and $Sm_{0.5}Sr_{0.5}CoO_3$ (SSC) at high temperatures over 1000 °C [51]. Fig. 5(c) shows the formation of $BaCoO_{2.23}$ at high temperatures and the peak shifts of BSCF at 1100 °C toward lower 2 theta, indicating the formation of A-site excess BSCF perovskite [52]. The oxygen-deficient barium cobaltate perovskite has a high oxygen permeability and a mixed ionic and electronic conductivity, but the severe interfacial chemical reactions to transform BSCF to $BaCoO_{2.23}$ at temperatures above 900–1000 °C as shown in Fig. 5 should be avoided to keep the electrochemical performance of BSCF cathode [53]. Further detailed interfacial electrochemical performance should be investigated to understand any beneficial or detrimental effects from the reacted interfaces.

Therefore, it was determined that the chemical reactions between BCZY and BSCF at high temperatures over 900 °C produced $BaCoO_{2.23}$ cubic perovskite, A-site cation-deficient BCZY, and A-site cation-excess BSCF. Even if Y or Zr in B-site of BCZY can be also partially diffused to BSCF, the peaks shift toward higher 2 theta indicative of the formation of B-site cation-rich BSCF weren't observed except for the BSCF peaks at 900 °C in Fig. 5(a) and (c). The solid solubility of Y or Zr with a larger ionic radius than Co or Fe in cubic BSCF perovskite would be very limited because the tolerance factor to keep cubic perovskite structure is in the range of 0.9–1.0. In addition, Co and Fe ions have almost the same size; therefore, the change of Co/Fe ratios in BSCF perovskite due to the formation of $BaCoO_{2.23}$ cubic perovskite at the interface with BCZY cannot cause any distinctive peak shifts of BSCF [54].

3.3. Evaluation of single cell performance under fuel cell and electrolysis modes

Fig. 6 shows the electrochemical performance of single cells composed of BSCF–BCZY cathode//BCZY electrolyte//NiO–BCZY anode as well as BCY-based materials at the temperature 600 °C under humid 75% H_2 in Ar (2.76% H_2O) as the fuel gas and humid air as the oxidant gas at a flow rate of 100 ml min^{-1}, respectively. The effective area of the cathode was 0.28 cm^{-2}. The effect of fabrication processing on cell performance was significant because the power densities of BCY electrolyte-based single cells fabricated by co-pressing and wet powder spraying were 140 and 225 mW cm^{-2} at 0.702 and 0.707 V, respectively and 600 °C. The BCZY-based single cell fabricated by wet powder spraying exhibited 493 mW cm^{-2} at 0.701 V and 600 °C. The fuel utilization and oxidant utilization at the power density with the current density of 708 mA cm^{-2} were 1.86 and 3.48%, respectively. The maximum power density of the single cell was slightly over 0.5 W cm^{-2} at 600 °C as shown in Fig. 6. To the best of authors' knowledge, the above mentioned maximum power density of 0.5 W cm^{-2} at 600 °C is the highest value from any planar type single cells with high temperature proton conducting electrolytes as thin as a few tens of micrometers [30,32,51].

Fig. 7 shows the open circuit voltages of single cells based on BCY and BCZY as a function of fuel gas flow rate at 600 °C. The open circuit voltages of 1.12–1.13 V obtained from the BCZY-based single

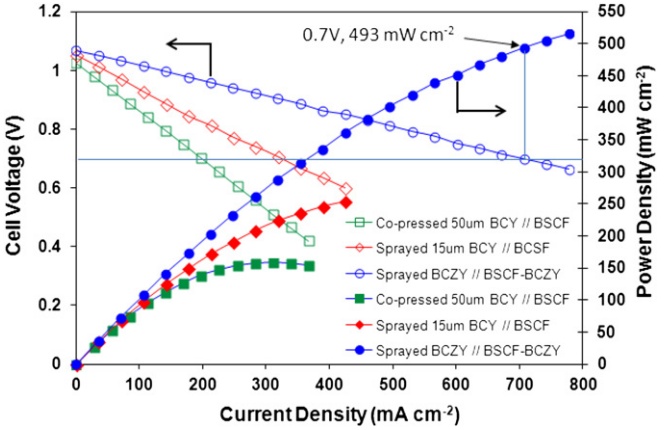

Fig. 6. I–V characteristics of single cells prepared by different fabrication processes and electrolyte materials at 600 °C under humid 75% H_2 in Ar (2.76% H_2O) and humid air.

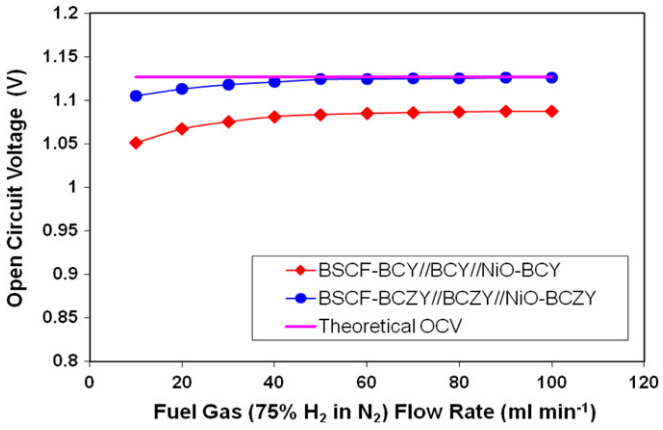

Fig. 7. Open circuit voltages of single cells based on BCY and BCZY under humid 75% H_2 in Ar (2.76% H_2O) as fuel and humid air (2.76% H_2O) as oxidant as a function of fuel gas flow rate at 600 °C.

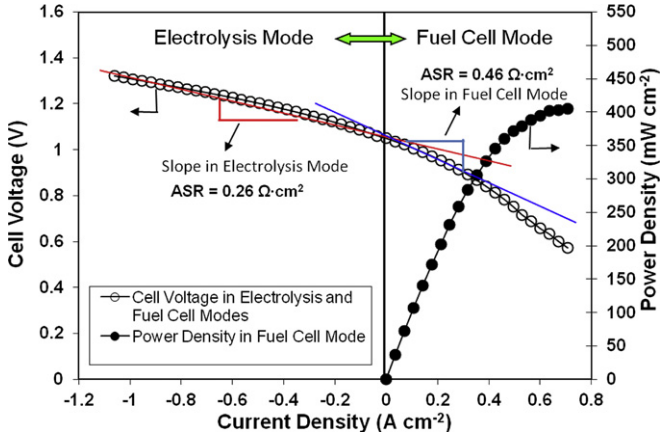

Fig. 9. Performance of a BCZY-based single cell in both fuel cell and electrolysis modes at 600 °C under humid air (2.76% H_2O) at the air electrode and humid 50% H_2 in Ar (2.76% H_2O) at the hydrogen electrode with a gas flow rate of 120 ml min^{-1}, respectively with the ASR calculation using the area of the air electrode.

cell at the fuel gas flow rates of 30–100 ml min^{-1} were very close to the theoretical value of 1.13 V calculated from the Nernst equation, indicating negligible gas leakage through the electrolyte. The slightly lowered open circuit voltages at the fuel gas flow rate less than 50 ml min^{-1} would be more related to the mechanical compressive seal of Ag for the single cell test fixture and alumina cement sealant used for fixing a single cell on a ceramic cell adapter developed in-house at NRC-EME. Fig. 8 shows the durability of a BCZY-based single cell at 600 °C under humid 75% H_2 in Ar as fuel and humid air as oxidant. The cell performance was relatively stable during the period of the test (up to 600 h) even if initial unstable voltage output related to cathode activation was observed. The durability of the BCZY-based single cell was very encouraging for practical use in fuel cells, but another critical checking point for applications would be its performance stability during thermal cycling as well as under hydrocarbon and/or sulfur-containing gas atmospheres. Especially the stability issue during thermal cycling is discussed in the next session.

In order to investigate the potential production of hydrogen via high temperature steam electrolysis using BCZY thin film electrolyte-based cells as shown in Fig. 9, an anode-supported button type single cell comprising of a 10–15 μm thick BCZY electrolyte, BSCF–BCZY air electrode and Ni–BCZY hydrogen electrode was electrochemically characterized in both of fuel cell and electrolysis modes. As shown in Fig. 9, the single cell exhibited good reversibility across the open-circuit voltage from the fuel cell mode to the electrolysis mode and much lower area-specific resistance in the electrolysis mode than that in the fuel cell mode based on the current density calculated by using the area of the air electrode that was one third of the area of the hydrogen electrode. The area specific resistances of 0.46 Ω cm^2 and 0.26 Ω cm^2 were obtained at 600 °C in the fuel cell reaction and electrolysis modes, respectively.

Based on the observation in the ASR measurement, it seems that the BSCF cathode can oxidize H_2O to produce O_2 and proton at the interface with a sufficient rate. The production rates of hydrogen at the cathode and oxygen at the anode in the electrolysis mode were monitored at a current density of 1050 mA cm^{-2} by using a multi-channel mass spectrometer. The theoretical production rate calculated from Faraday's law is approximately 7.3 ml min^{-1} cm^{-2} at the current density. The measured hydrogen evolution rate at the fuel electrode was 7.1 ml min^{-1} cm^{-2}, but gradually decreased due to the low partial pressure of water vapor of approximate 0.03 atm in the humid air supplied at the anode. This result can be considered very encouraging because the BSCF–BCZY composite anode exhibits high reaction kinetics of H_2O oxidation during the high temperature steam electrolysis.

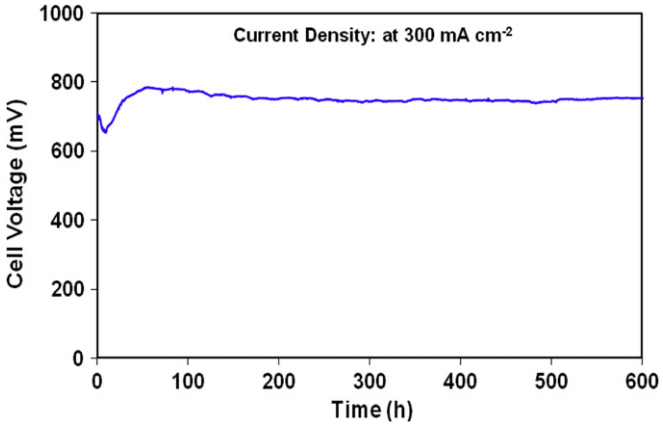

Fig. 8. Degradation of a single cell of BSCF–BCZY//BCZY//NiO–BCZY at 600 °C under humid 75% H_2 in Ar (2.76% H_2O) as fuel and humid air as oxidant with gas flow rates of 50 and 100 ml min^{-1}, respectively.

3.4. Chemical stability of BCZY electrolyte under humid atmosphere

The stability of BCZY electrolyte in water-containing atmospheres was investigated by exposing sintered BCZY pellets to humid air (2.76% H_2O) at 200 °C for 24 h or boiling them in water for 3 h in order to enhance understanding about potential problematic degradation issues during thermal cycling under humid gas atmosphere. The thermal cycling of BCZY-based cells is inevitable for long term operation in any practical applications. Even if the single cell showed good short-term durability as shown in Fig. 8, it can be exposed to highly humid atmosphere during thermal cycling, especially at low temperatures below 200 °C. The stability of BCZY under H_2O-containing atmosphere at low temperatures would be much more critical than *C–V* characteristics and durability tested at high temperatures for practical applications because Bhide and Virkar reported that undoped, Gd-doped, and La-doped $BaCeO_3$ ceramics at all dopant levels were readily decomposed within a few hours when boiled in water and some of the powders were decomposed when heated in moist air at 200 °C after several days of exposure [15]. During thermal cycling, BCZY electrolyte can

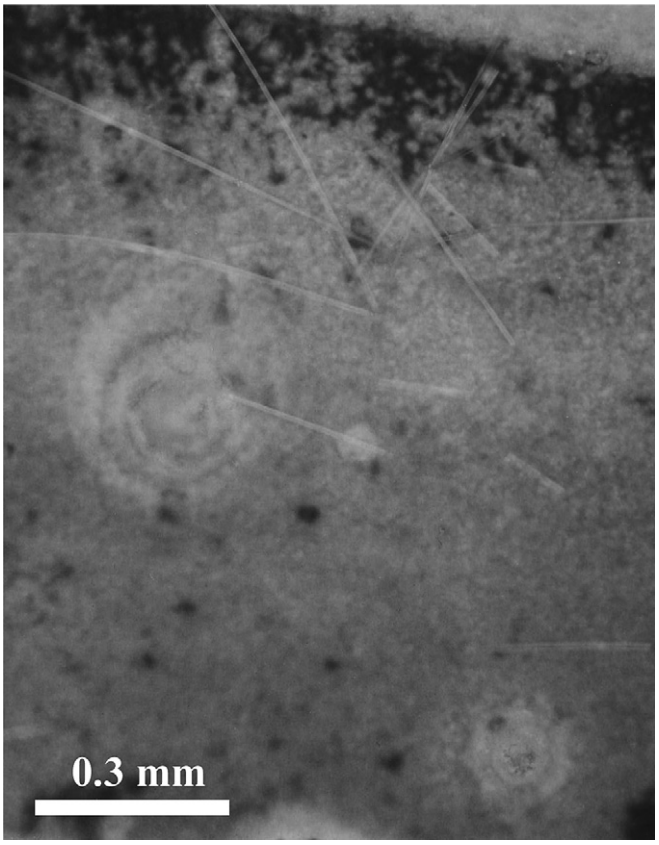

Fig. 10. Optical microscopic image (×100) of the surface of thin BCZY electrolyte deposited on a single cell after cooling from a high temperature steam electrolysis test at 600 °C under humid gas atmosphere.

be damaged from residual H_2O in the electrolyte layer at low temperatures even after purging with dry gas on the cells and stacks. Therefore, it's very interesting to investigate the chemical stability of BCZY under humid air (2.76% H_2O) at 200 °C or in boiling water for practical applications.

Fig. 10 shows an optical microscopic image (×100) of the surface of thin BCZY electrolyte deposited on a single cell after cooling from a high temperature steam electrolysis test at 600 °C. The surface of the BCZY electrolyte was covered with white color, thin-film deposit and whiskers that would be mainly comprised of barium carbonate and barium hydroxide. In order to determine the phase formed on the electrolyte, a sintered BCZY pellet was heat-treated at 200 °C for 24 h under humid air with a gas flow rate of 100 ml min^{-1} in a 2″ diameter tubular furnace and its surface was examined by SEM/EDX as shown in Fig. 11. The surface of the BCZY pellet heat-treated at 200 °C for 24 h under humid air has some regions reacted with H_2O and CO_2 in the purging gas as shown in Fig. 11(b) and (c). The elemental analysis for the five selected areas on the sintered BCZY pellet shown in Fig. 11(d) was summarized in Table 1.

As shown in Fig. 11(a), the BCZY pellet sintered at 1500 °C without any additives has much porous microstructure in comparison to thin-film BCZY supported on NiO–BCZY shown in Fig. 3. Therefore, it was proven that Ni diffusion from anode support to BCZY electrolyte was very effective to enhance the densification of BCZY electrolyte during co-firing. The BCZY surface reacted with H_2O and CO_2 in the purging gas formed 3 different type reaction products including spherical shape carbonate-rich deposit, barium carbonate-based bar type deposit, and cerium oxide-rich planar layer deposit as shown in Fig. 11(d) and summarized in Table 1. The accumulated reaction products formed during thermal cycling may result in significant degradation of cell performance. The chemical reaction of BCZY to form barium carbonate and barium hydroxide

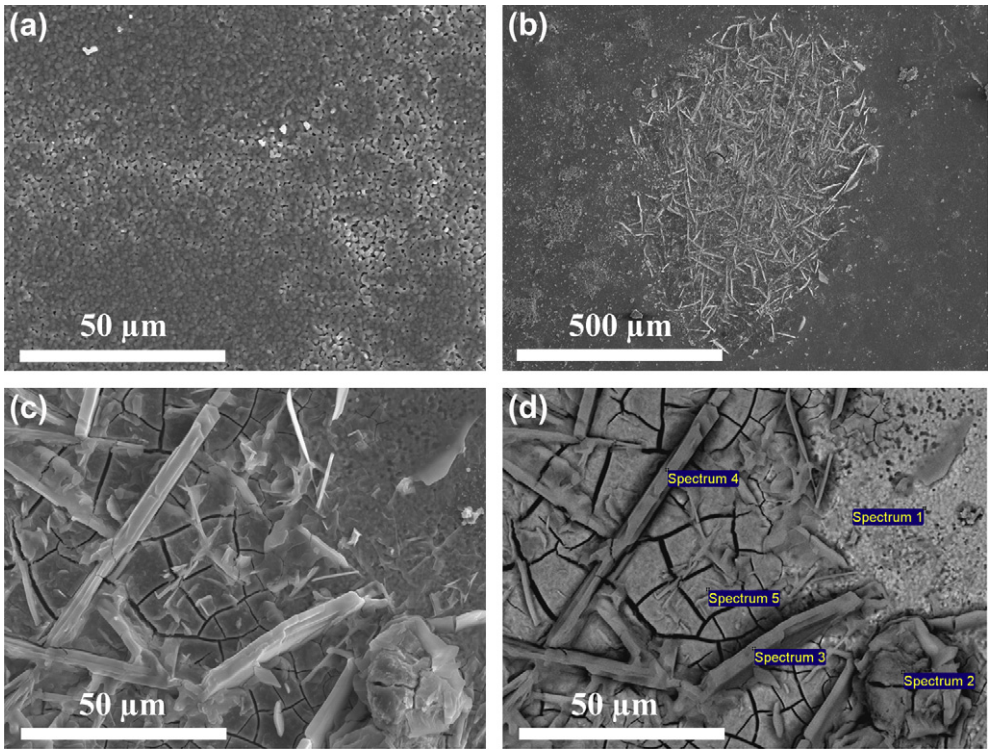

Fig. 11. Scanning electron micrographs of the surface morphology of BCZY electrolyte pellets (a) as sintered at 1500 °C, (b) After heating at 200 °C for 24 h under humid air (a low magnification), (c) After heating at 200 °C for 24 h under humid air (a high magnification), and (d) as a backscattered electron image of (c) for elemental analysis by EDX.

Table 1
Elemental analysis for 5 selected areas on a sintered BCZY pellet after heating at 200 °C for 24 h under humid air.

Location	Ba	Ce	Zr	Y	O	C (atomic %)	Remarks
BCZY	20.00	12.00	4.00	4.00	60.00	–	Calculated
Spectrum 1	23.23	12.84	3.49	2.99	57.45	–	Unreacted zone
Spectrum 2	5.99	3.28	1.28	1.31	78.94	9.20	Reacted: round deposit
Spectrum 3	18.32	0.96	0.41	0.44	65.85	14.01	Reacted: bar type deposit
Spectrum 4	15.26	0.35	0.00	0.00	67.17	17.22	Reacted: bar type deposit
Spectrum 5	23.29	17.61	3.80	3.47	51.83	–	Reacted: ceria-rich layer

can happen via reactions with H_2O and CO_2 in the gases as well as with residual H_2O in the electrolyte during cooling; therefore, it seems that the composition of $Ba_{0.98}Ce_{0.6}Zr_{0.2}Y_{0.2}O_{3-\delta}$ tested in this study should be modified by increasing Zr concentration to enhance the stability in water-containing atmospheres at low temperatures.

Fig. 12 shows the X-ray diffraction patterns of sintered BCZY pellets heat-treated at 200 °C for 24 h under humid air and soaked in boiling water for 3 h. Fig. 12(b) clearly shows the formation of $BaCO_3$ as well as $Ba(OH)_2$ on the BCZY surface during heating at 200 °C for 24 h under humid air. In addition, the surface of a sintered BCZY pellet soaked in boiling water for 3 h formed barium carbonate, barium hydroxide, and cerium zirconate as shown in Fig. 12(a). The reacted products formed at 200 °C under humid air or in boiling water can be produced by the following Eqs. (5)–(7).

$$Ba(Ce_{0.6}Zr_{0.2}Y_{0.2})O_{2.9} + H_2O = Ba(OH)_2 + 0.8(Ce_{0.75}Zr_{0.25})O_2 + 0.1Y_2O_3 \quad (5)$$

$$Ba(OH)_2 + CO_2 = BaCO_3 + H_2O \quad (6)$$

$$Ba(Ce_{0.6}Zr_{0.2}Y_{0.2})O_{2.9} + CO_2 = BaCO_3 + 0.8(Ce_{0.75}Zr_{0.25})O_2 + 0.1Y_2O_3 \quad (7)$$

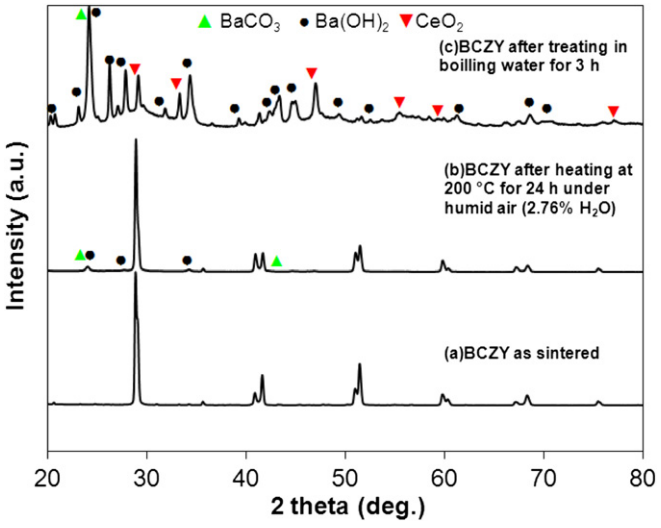

Fig. 12. XRD patterns of sintered BCZY pellets heat-treated under different conditions.

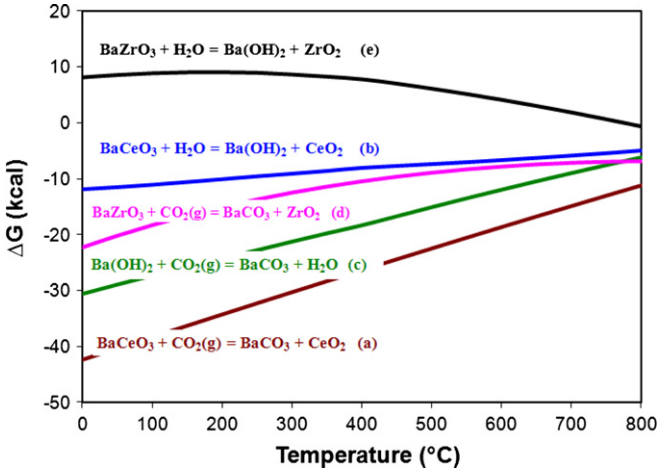

Fig. 13. Thermodynamics of chemical reactions of $BaCeO_3$ and $BaZrO_3$ under CO_2 and H_2O as a function of temperatures.

Fig. 13 shows thermodynamics of chemical reactions of $BaCeO_3$ and $BaZrO_3$ under CO_2 and H_2O, calculated using HSC-Chemistry 5 software. As can be seen, the values of Gibbs free energy change of the reaction (e) are positive in the temperature range of 0–750 °C, indicating that the reaction (e) has difficulty in occurring under conditions studied. Therefore, the further increase of Zr concentration incorporated in $Ba_{0.98}Ce_{0.6}Zr_{0.2}Y_{0.2}O_{3-\delta}$ can significantly enhance the chemical stability under water-containing atmospheres, but the high Zr concentration in the BCZY electrolyte would reduce its sinterability. The further optimization to select Zr concentration in BCZY and its desirable sintering temperature should be performed based on the densification of the thin-film BCZY electrolyte supported by NiO-based anode, electrochemical cell performance, and the stability of the electrolyte under water-containing atmosphere during thermal cycling as well as under CO_2- and H_2S-containing atmospheres at operating temperatures.

4. Conclusions

The high performance anode supported single cells, comprising of BSCF–BCZY//BCZY ($Ba_{0.98}Ce_{0.6}Zr_{0.2}Y_{0.2}O_{3-\delta}$)//NiO–BCZY have been fabricated by wet powder spraying and co-firing for depositing 10–15 μm thin film electrolytes on pre-sintered NiO–BCZY anode discs for a variety of applications such as humid hydrogen or potentially ammonia fuelled proton conducting solid oxide fuel cells (SOFCs) and high temperature steam electrolysis as reversible SOFCs. BCZY has higher resistance to Ni diffusion, resulting in the formation of the secondary phase of BaY_2NiO_5 than BCY at high temperatures.

It was possible to increase the sintering temperature of BCZY electrolyte deposited on NiO–BCZY anode up to 1350–1400 °C for producing dense BCZY thin-film electrolyte without the formation of any visible secondary phase on the surface of the BCZY electrolyte to fabricate high performance anode-supported BCZY-based single cells. The chemical reactions between BCZY and BSCF at high temperatures over 900 °C produced $BaCoO_{2.23}$ cubic perovskite, A-site cation-deficient BCZY, and A-site cation-excess BSCF. Even if the oxygen-deficient barium cobaltate perovskite has a high oxygen permeability and a mixed ionic and electronic conductivity, the severe interfacial chemical reactions to transform BSCF to $BaCoO_{2.23}$ at temperatures above 900–1000 °C should be avoided to keep the electrochemical performance of BSCF cathode.

The electrochemical performance of single cells was characterized at the temperature 600–700 °C under humid 50–75% H_2 in N_2 (2.76% H_2O) as the fuel gas and humid air as the oxidant gas at a gas flow rate of 10–100 ml min^{-1}. The open circuit voltages were around 1.12–1.13 V at 600 °C indicating negligible gas leakage or mixed conduction through the electrolyte. The maximum power density of 493 mW cm^{-2} was obtained at 600 °C and 0.7 V under humid air as the oxidant gas and humid 75% H_2 in N_2 (2.76% H_2O) as the fuel gas at a gas flow rate of 100 ml min^{-1}. The area specific resistance of an anode supported button cell of BSCF–BCZY//BCZY//NiO–BCZY in fuel cell mode was about 0.46 Ω cm^2 and in the electrolysis mode was 0.26 Ω cm^2 at 600 °C, indicating high efficiency, reversible SOFCs. The single cell performance was stable for over 600 h at 600 °C.

The stability of BCZY electrolyte in water-containing atmospheres was investigated by exposing sintered BCZY pellets to humid air (2.76% H_2O) at 200 °C for 24 h or soaking them in boiling water for 3 h. The BCZY surface reacted with H_2O and CO_2 in the purging gas formed 3 different type reaction products including spherical shape carbonate-rich deposit, barium carbonate-based bar type deposit, and cerium oxide-rich planar layer deposit. In addition, XRD analysis clearly showed the formation of $BaCO_3$ as well as $Ba(OH)_2$ on the BCZY surface during heating at 200 °C for 24 h under humid air. The surface of a sintered BCZY pellet soaked in boiling water for 3 h formed barium carbonate, barium hydroxide, and cerium zirconate.

Therefore, the composition of $Ba_{0.98}Ce_{0.6}Zr_{0.2}Y_{0.2}O_{3-\delta}$ tested in this study should be modified by increasing Zr concentration to enhance the stability in water-containing atmospheres at low temperatures. The further optimization to select Zr concentration in BCZY and its desirable sintering temperature should be performed based on the densification of the thin-film BCZY electrolyte supported by NiO-based anode, electrochemical cell performance, and the stability of the electrolyte under water-containing atmosphere during thermal cycling as well as under CO_2- and H_2S-containing atmospheres at operating temperatures.

Acknowledgments

This work was financially supported by the Program of Energy Research and Development (PERD) Technology and Innovation (T&I) in Canada. The authors would like to gratefully acknowledge the assistance of Dr. A. McFarlan at Natural Resources Canada (NRCan)-CanmetENERGY. Thanks are also addressed to Mr. D. Kingston for SEM/EDX and Mr. Xiaohua Deng for sample preparation and XRD analysis.

References

[1] H. Iwahara, T. Esaka, H. Uchida, N. Maeda, Solid State Ionics 3/4 (1981) 359.
[2] H. Iwahara, H. Uchida, N. Maeda, J. Power Sources 7 (1982) 293.
[3] H. Iwahara, H. Uchida, K. Ono, K. Ogaki, J. Electrochem. Soc. 135 (2) (1988) 529.
[4] H. Iwahara, Solid State Ionics 28–30 (1988) 573.
[5] T. Kobayashi, K. Abe, Y. Ukyo, H. Matsumoto, Solid State Ionics 138 (2001) 243.
[6] N. Bonanos, B. Ellis, K.S. Knight, M.N. Mahmood, Solid State Ionics 35 (1989) 179.
[7] N. Taniguchi, K. Hatoh, J. Niikura, T. Gamo, Solid State Ionics 53–56 (1992) 998.
[8] Y. Yoo, M. Tuck, N. Lim, A. McFarlan, N. Maffei, ECS Trans. 7 (1) (2007) 2305.
[9] V. Agarwal, M. Liu, J. Electrochem. Soc. 144 (3) (1997) 1035.
[10] S. Gopalan, A.V. Virkar, J. Electrochem. Soc. 140 (4) (1993) 1060.
[11] M.J. Scholten, J. Schoonman, Solid State Ionics 61 (1993) 83.
[12] N. Bonanos, K.S. Knight, B. Ellis, Solid State Ionics 79 (1995) 161.
[13] C.W. Tanner, A.V. Virkar, J. Electrochem. Soc. 143 (4) (1996) 1386.
[14] Z. Wu, M. Liu, J. Electrochem. Soc. 144 (6) (1997) 2170.
[15] S.V. Bhide, A.V. Virkar, J. Electrochem. Soc. 146 (6) (1999) 2038.
[16] S. Wienströer, H.-D. Wiemhöfer, Solid State Ionics 101 (1997) 1113.
[17] K.H. Ryu, S.M. Haile, Solid State Ionics 125 (1999) 355.
[18] N. Taniguchi, C. Nishimura, J. Kato, Solid State Ionics 145 (2001) 349.
[19] N. Osman, I.A. Talib, H.A. Hamid, Ionics 16 (2010) 561.
[20] S. Barison, M. Battagliarin, T. Cavallin, L. Doubova, M. Fabrizio, C. Mortalo, S. Boldrini, L. Malavasi, R. Gerbasi, J. Mater. Chem. 18 (2008) 5120.
[21] K. Katahira, Y. Kohchi, T. Shimura, H. Iwahara, Solid State Ionics 138 (2000) 91.
[22] Z. Zhong, Solid State Ionics 178 (2007) 213.
[23] S. Ricote, N. Bonanos, M.C. Marco de Lucas, G. Caboche, J. Power Sources 193 (2009) 189.
[24] J. Li, J. Luo, K.T. Chuang, A.R. Sanger, Electrochim. Acta 53 (2008) 3701.
[25] J. Lv, L. Wang, D. Lei, H. Guo, R.V. Kumar, J. Alloys Compd. 467 (2009) 376.
[26] R.D. Shannon, Acta Cryst A32 (1976) 751.
[27] C. Zuo, S. Zha, M. Liu, M. Hatano, M. Uchiyama, Adv. Mater. 18 (2006) 3318.
[28] E. Fabbri, A. D'Epifanio, E. Di Bartolomeo, S. Licoccia, E. Traversa, Solid State Ionics 179 (2008) 558.
[29] Y. Yoo, N. Lim, 8th Eur. SOFC Forum, Lucerne, Switzerland, p. A1106, 2008.
[30] Y. Guo, Y. Lin, R. Ran, Z. Shao, J. Power Sources 193 (2009) 400.
[31] Y. Lin, R. Ran, Y. Guo, W. Zhou, R. Cai, J. Wang, Z. Shao, Int. J. Hydrogen Energy 35 (2010) 2637.
[32] F. He, D. Song, R. Peng, G. Meng, S. Yang, J. Power Sources 195 (2010) 3359.
[33] N. Oishi, Y. Yoo, I. Davidson, J. Am. Ceram. Soc. 90 (5) (2007) 1365.
[34] J. Amador, E. Gutierrez Puebla, M.A. Monge, I. Rasines, J.A. Campa, J.M. Gomez de Salazar, C. Ruiz Valero, Solid State Ionics 32–33 (1989) 123.
[35] Y. Yoo, N. Lim, M. Phongakson, A. McFarlan, N. Maffei, ECS Trans. 12 (1) (2008) 691.
[36] J. Tong, D. Clark, L. Bernau, A. Subramaniyan, R. O'Hayre, Solid State Ionics 181 (2010) 1486.
[37] J. Tong, D. Clark, L. Bernau, M. Sanders, R. O'Hayre, J. Mater. Chem. 20 (2010) 6333.
[38] N. Zakowsky, S. Williamson, J.T.S. Irvine, Solid State Ionics 176 (2005) 3019.
[39] J. Ovenstone, J.-I. Jung, J.S. White, D.D. Edwards, S.T. Misture, J. Solid State Chem. 181 (2008) 576.
[40] H. Wang, C. Tablet, W. Yang, J. Caro, Mater. Lett. 59 (2005) 3750.
[41] P. Haworth, S. Smart, J. Glasscock, J.C. Diniz da Costa, Sep. Purif. Technol. 81 (2011) 88.
[42] P. Haworth, S. Smart, J. Glasscock, J.C. Diniz da Costa, Sep. Purif. Technol. 94 (2012) 16.
[43] P.F. Haworth, S. Smart, J.M. Serra, J.C. Diniz da Costa, Phys. Chem. Chem. Phys. 14 (2012) 9104.
[44] X. Meng, N. Yang, B. Meng, X. Tan, Z.-F. Ma, S. Liu, Ceram. Int. 37 (2011) 2701.
[45] H. Lu, Z. Deng, J. Tong, W. Yang, Mater. Lett. 59 (2005) 2285.
[46] Y. Lin, R. Ran, Y. Zheng, Z. Shao, W. Jin, N. Xu, J. Ahn, J. Power Sources 180 (2008) 15.
[47] J. Wu, L.P. Li, W.T.P. Espinosa, S.M. Haile, J. Mater. Res. 19 (8) (2004) 2366.
[48] J. Wu, R.A. Davies, M.S. Islam, S.M. Haile, Chem. Mater. 17 (2005) 846.
[49] D. Shima, S.M. Haile, Solid State Ionics 97 (1997) 443.
[50] S.W. Strauss, I. Fankuchen, R. Ward, J. Am. Chem. Soc. 73 (1951) 5084.
[51] L. Yang, C. Zuo, S. Wang, Z. Cheng, M. Liu, Adv. Mater. 20 (2008) 3280.
[52] W. Zhou, R. Ran, Z. Shao, W. Zhuang, J. Jia, H. Gu, W. Jin, N. Xu, Acta Materialia 56 (2008) 2678.
[53] T. Ishihara, S. Fukui, H. Nishiguchi, Y. Takita, J. Electrochem. Soc. 149 (7) (2002) A823.
[54] E.A. Kotomin, R. Merkle, Y.A. Mastrikov, M.M. Kuklja, J. Maier, ECS Trans. 35 (1) (2011) 823.